Open access • Report • DOI:10.2172/6789158

Three-dimensional MHD (magnetohydrodynamic) flows in rectangular ducts of liquid-metal-cooled blankets — Source link ↗

T.Q. Hua, B.F. Picologlou, C.B. Reed, John S. Walker

Related papers:

- Self-cooled liquid-metal blanket concept

- A parametric study of 3D mhd flows in expansions of rectangular ducts

- Buoyant flow in long vertical enclosures in the presence of a strong horizontal magnetic field. Part 2. Finite enclosures

- Magnetohydrodynamic Flow in a Manifold and Multiple Rectangular Coolant Ducts of Self-Cooled Blankets

- Blanket Comparison and Selection Study

ANL/FPP/TM-228

Argonne National Laboratory
9700 South Cass Avenue
Argonne, Illinois 60439

THREE-DIMENSIONAL MHD FLOWS IN RECTANGULAR DUCTS
OF LIQUID-METAL-COOLED BLANKETS

T. Q. Hua, J. S. Walker, B. F. Picologlou, and C. B. Reed

July 1988

CONTENTS

LIST OF FIGURES

THREE-DIMENSIONAL MHD FLOWS IN RECTANGULAR DUCTS OF LIQUID-METAL-COOLED BLANKETS

T. Q. Hua, J. S. Walker, B. F. Picologlou, and C. B. Reed

ABSTRACT

Magnetohydrodynamic flows of liquid metals in rectangular ducts with thin conducting walls in the presence of strong nonuniform transverse magnetic fields are examined. The interaction parameter and Hartmann number are assumed to be large, whereas the magnetic Reynolds number is assumed to be small. Under these assumptions, viscous and inertial effects are confined in very thin boundary layers adjacent to the walls. A significant fraction of the fluid flow is concentrated in the boundary layers adjacent to the side walls which are parallel to the magnetic field. This paper describes the analysis and numerical methods for obtaining 3-D solutions for flow parameters outside these layers, without solving explicitly for the layers themselves. Numerical solutions are presented for cases which are relevant to the flows of liquid metals in fusion reactor blankets. Experimental results obtained from the ALEX experiments at Argonne National Laboratory are used to validate the numerical code. In general, the agreement is excellent.

1.0   INTRODUCTION

In a self-cooled liquid-metal blanket for a magnetically confined fusion reactor, the magnetohydrodynamic (MHD) effects are of paramount importance in the design process [1]. The interaction between the circulating liquid metal with the strong toroidal magnetic field results in large electromagnetic body forces which determine the flow distribution of the liquid metal, and produce large MHD pressure gradients. The resulting MHD pressure drop may cause excessive pumping power loss and large material stresses. Also, the MHD flow distribution may affect drastically the heat transfer characteristics of the blanket in general and the first wall coolant channels in particular.

An experimental and analytical program is being carried out at Argonne National Laboratory (ANL) to investigate the MHD effects in liquid metal flows in electrically conducting conduits of various geometries. Experiments are conducted in the Argonne Liquid Metal Experiment (ALEX) facility [2]. A recent summary of the experiments and code development efforts for a round duct and a rectangular duct can be found in Reference 3. This paper concentrates on the theoretical analysis and the numerical methods for a straight rectangular duct, with applications to a fusion blanket module. Some representative experimental data obtained through the ALEX experiments are presented for comparison with the numerical predictions.

2.0   THEORETICAL CONSIDERATIONS

2.1   Formulation of the Problem

We consider the steady flow of an incompressible liquid metal driven by a pressure gradient along a rectangular duct with thin metal walls and with an imposed transverse magnetic field whose strength varies along the duct (Figure 1). A transverse magnetic field variation in the axial direction requires a non-zero axial magnetic field. This weaker axial magnetic field is neglected in this model because the major magnetic body force in the liquid metal arises from the interaction between the fluid flow with the transverse field. The ratio of the induced to applied fields is given by $c^{1/2} R_m$. Here,

$$c = \frac{\sigma_w t}{\sigma L}$$
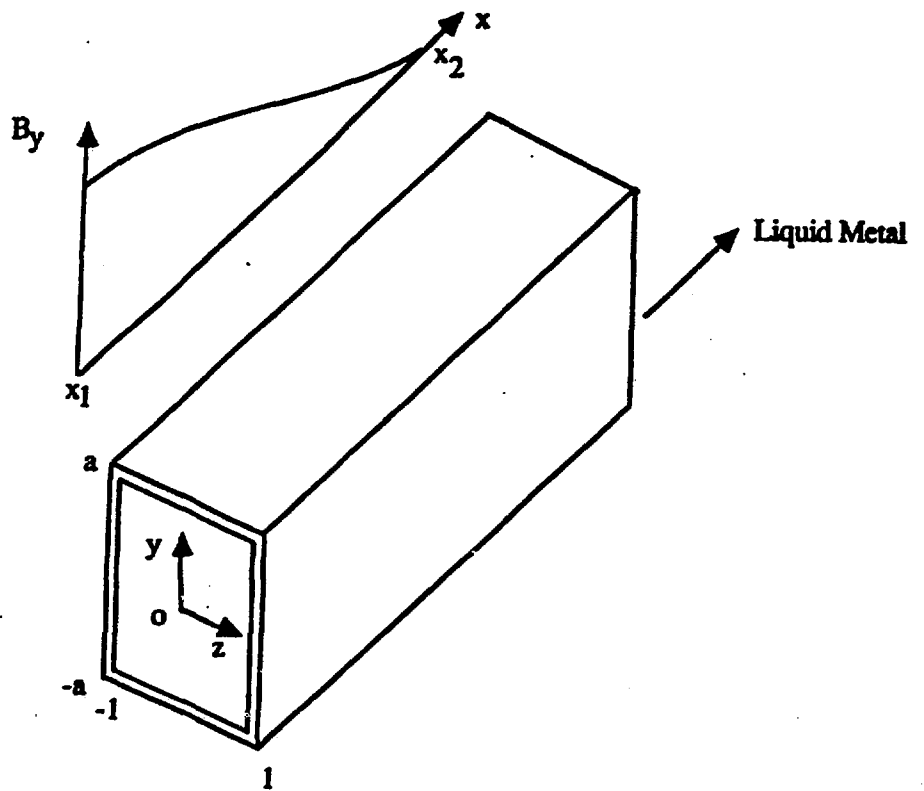
$$R_m = \mu \sigma U L$$

FIGURE 1. SCHEMATIC DIAGRAM OF THE PHYSICAL MODEL

are the wall conductance ratio and magnetic Reynolds number. μ and σ are the magnetic permeability and electrical conductivity of the liquid metal, σ_w and t are the electrical conductivity and thickness of the duct wall, U_0 is the average axial velocity of the fluid and L is a characteristic transverse dimension of the duct. For a self-cooled blanket in a fusion device, $c^{1/2} R_m$ is at most of order 10^{-2}; therefore, it is appropriate to neglect the induced field.

Neglecting induction, the magnetic field $\underset{\sim}{B}$ satisfies

$$\underset{\sim}{\nabla} \cdot \underset{\sim}{B} = 0,$$

$$\underset{\sim}{\nabla} \times \underset{\sim}{B} = 0.$$

We consider plane fields, $\underset{\sim}{B} = B_x (x,y) \underset{\sim}{\hat{x}} + B_y (x,y) \underset{\sim}{\hat{y}}$, where $\underset{\sim}{\hat{x}}$ and $\underset{\sim}{\hat{y}}$ are unit vectors. We assume that $\underset{\sim}{B}$ is symmetric about the y = 0 plane and that $\underset{\sim}{B}$ varies in the x direction over a characteristic axial length $L_B \gg L$. Then the solution for $\underset{\sim}{B}$ is

$$\underset{\sim}{B} = B_y(x) \underset{\sim}{\hat{y}}$$

neglecting $O(L/L_B)$ terms.

For this problem we assume the same conductance ratio, c_t, for the top and bottom walls (perpendicular to the magnetic field $\underset{\sim}{B}$), and the same conductance ratio, c_s, for the side walls (parallel to $\underset{\sim}{B}$). By symmetry, the solution is sought in one quadrant of the duct, namely for $0 \leq y \leq a$, $-1 \leq z \leq 0$ (all lengths are nondimensionalized by L, half the distance between the side walls). The present analysis can be extended in a straightforward manner to treat the entire duct with unequal conductance ratios on all walls, as well as varying conductance ratio along the length.

The two important parameters in any general MHD problem are the interaction parameter, N, and Hartmann number, M, defined by

$$N = \frac{\sigma B_0^2 L}{\rho U_0}$$

$$M = L B_0 \left(\frac{\sigma}{\rho \nu} \right)^{1/2}$$

where ρ and ν are the fluid's density and kinematic viscosity, respectively, and B_0 is a characteristic magnetic flux density. The interaction parameter represents the ratio of the electromagnetic (EM) force to the inertia body force, and the Hartmann number represents the square root of the ratio of EM force to the viscous body force. The values for M and N in a tokamak reactor are typically of the order of $10^3 - 10^5$[1]. This means that the EM force is the dominant force determining the flow and pressure distributions throughout the liquid-metal flow, except for thin boundary and possibly free shear layers. Outside these layers, the 3-D distributions of the flow parameters (velocities, electric current densities, electric potential and pressure) can be derived from two classes of scalar functions of two space variables. The functions are the pressure in the fluid and the electric potential at the walls.

The inertialess, inviscid, dimensionless equations governing the flow of a liquid metal in the core of the flow are:

$$\nabla p = \underset{\sim}{j} \times \underline{B} \tag{1a}$$

$$\underset{\sim}{j} = - \nabla \phi + \underset{\sim}{v} \times \underline{B} \tag{1b}$$

$$\nabla \cdot \underset{\sim}{v} = 0 \tag{1c}$$

$$\nabla \cdot \underset{\sim}{j} = 0 . \tag{1d}$$

Here p, j, $\underset{\sim}{v}$, and ϕ are the pressure, electric current density, velocity, and electric potential, normalized by $\sigma U_0 B_0^2 L$, $\sigma U_0 B_0$, U_0, and $U_0 B_0 L$, respectively. For $N = 10^4$, $M = 10^4$, and $c = 0.01$, and in the core where $\underset{\sim}{v} = O(1)$, $\underset{\sim}{v} = O(1)$, the errors associated with the inertialess and inviscid assumptions are of order $N^{-1} c^{1/2} = 10^{-3}$ and $M^{-2} c^{-1} = 10^{-6}$.

The x,y,z core velocity components u_c, v_c, w_c, and electric current density components j_{xc}, j_{yc}, j_{zc}, which satisfy the equations (1) and the symmetry conditions, $j_{yc} = v_c = 0$ at $y = 0$, are:

$$u_c(x,y,z) = \beta \frac{\partial \phi_c}{\partial z} - \beta^2 \frac{\partial p}{\partial x} \tag{2a}, \text{(Cf. 1b)}$$

4

$$w_c(x,y,z) = -\beta \frac{\partial \phi_c}{\partial x} - \beta^2 \frac{\partial p}{\partial z} \qquad \text{(2b), (Cf. 1b)}$$

$$v_c(x,y,z) = -y\,\beta'(x)\,\frac{\partial \phi_t}{\partial z} + y\,\frac{\partial}{\partial x}\,[\beta^2 \frac{\partial p}{\partial x}]$$

$$+ y\,[\beta^2 + \frac{1}{2}\,(a^2 - \frac{y^2}{3})\,\beta'^2]\,\frac{\partial^2 p}{\partial z^2} \qquad \text{(2c), (Cf. 1c)}$$

$$j_{xc}(x,y,z) = \beta \frac{\partial p}{\partial z} \qquad \text{(2d), (Cf. 1a)}$$

$$j_{zc}(x,y,z) = -\beta \frac{\partial p}{\partial x} \qquad \text{(2e), (Cf. 1a)}$$

$$j_{yc}(x,y,z) = -y\beta' \frac{\partial p}{\partial z} \qquad \text{(2f), (Cf. 1d)}$$

where $p(x,z)$ is the pressure which is constant along magnetic field lines by virtue of Eq. (1a), $\beta(x) = B^{-1}_u(x)$, and $\beta' = d\beta/dx$. The electric potential in the core varies along the magnetic field lines according to

$$\phi_c(x,y,z) = \phi_t(x,z) - \frac{1}{2}\,(a^2 - y^2)\,\beta'\,\frac{\partial p}{\partial z}, \qquad \text{(2g)}$$

where $\phi_t(x,z)$ is the electric potential at the top wall at $y = a$. Equation (2g) is obtained by integrating the y- component of equation (1b), and using equation (2f).

2.2   Governing Equations

The three-dimensional problem with eight variables in the core (pressure, electric potential, three components of velocity and three components of current density) is completely solved once the functions $p(x,z)$ and $\phi_t(x,z)$ are determined. The equations necessary for the determination of $p(x,z)$ and $\phi_t(x,z)$ are provided by the boundary conditions. The boundary conditions at the inside surface of the top wall, at $y = a$, are:

5

$$v = 0 \tag{3a}$$

$$j_{yc} = -c_t \left[\frac{\partial^2 \phi_t}{\partial x^2} + \frac{\partial^2 \phi_t}{\partial z^2} \right] \qquad \text{at } y = a \tag{3b}$$

These conditions neglect the $O(M^{-1})$ jumps in v, j_y and ϕ across the Hartmann layer, which separates the inviscid core region from the top. Condition (3b), also known as the thin conducting wall condition, neglects terms which are $O(t^2/a^2)$ compared to those retained [4]. Neglecting $O(M^{-1/2})$, the jump across the side wall layer which has $O(M^{-1/2})$ thickness leads to the additional condition

$$j_{zc} = +c_s \left[\frac{\partial^2 \phi_s}{\partial x^2} + \frac{\partial^2 \phi_s}{\partial y^2} \right] \qquad \text{at } z = -1, \tag{3c}$$

where $\phi_s(x,y)$ is the electric potential at the side.

The conditions (3a) and (3b), when applied to equations (2c) and (2f), give two coupled partial differential equations governing $p(x,z)$ and $\phi_t(x,z)$:

$$\frac{\partial}{\partial x} \left[\beta^2 \frac{\partial p}{\partial x} \right] + \left[\beta^2 + \frac{a^2}{3} \beta'^2 \right] \frac{\partial^2 p}{\partial z^2} = \beta' \frac{\partial \phi_t}{\partial \epsilon} \tag{4a}$$

$$c_t \left[\frac{\partial^2 \phi_t}{\partial x^2} + \frac{\partial^2 \phi_t}{\partial z^2} \right] = a\beta' \frac{\partial p}{\partial z}. \tag{4b}$$

Likewise, condition (3c) applied to equation (2e) at $z = -1$ gives the governing equation for $\phi_s(x,y)$

$$c_s \left[\frac{\partial^2 \phi_s}{\partial x^2} + \frac{\partial^2 \phi_s}{\partial y^2} \right] = -\beta \frac{\partial p}{\partial x} (x, -1) \tag{4c}$$

2.3 Boundary Conditions

Sufficiently upstream and downstream of the region where the magnetic field is changing, the flow will be fully developed. For fully developed flow, there are no axial currents in the core or in the walls. The appropriate boundary conditions at the upstream cross section, x_1, and at the downstream cross section, x_2, are:

6

$$p = p_1$$

$$\frac{\partial \phi_t}{\partial x} = \frac{\partial \phi_s}{\partial x} = 0 \qquad \text{at } x = x_1, \qquad\qquad (5a,b,c)$$

and

$$p = p_2$$

$$\frac{\partial \phi_t}{\partial x} = \frac{\partial \phi_s}{\partial x} = 0 \qquad \text{at } x = x_2. \qquad\qquad (5d,e,f)$$

The constants p_1 and p_2 ($p_1 > p_2$) can be arbitrarily chosen. After the solution is found, every variable is multiplied by a scaling factor to get the desired volumetric flux. The dimensionless axial velocity must satisfy the total volumetric condition

$$\int_o^a \int_{-1}^o u(x,y,z)\, dydz = a \qquad\qquad (6)$$

at every cross section. Initially, we choose $p_1 = 1$ and $p_2 = 0$. Then each variable is multiplied by the correct value of p_1 which is given by the ratio of "a" to the integral of the initial u over a quarter cross section.

Additional boundary conditions are provided by symmetry about the $z = 0$ and $y = 0$ planes, namely:

$$\phi_t = 0$$

$$\frac{\partial p}{\partial z} = 0 \qquad \text{at } z = 0,$$

and

$$\frac{\partial \phi_s}{\partial y} = 0 \qquad \text{at } y = 0. \qquad\qquad (7a,b,c)$$

Finally, we must also ensure that electric potential and electric current density are continuous at the corner $y = a$ and $z = -1$. This requires that

7

$$\phi_t \ (x, -1) = \phi_s \ (x,a) \tag{7d}$$

$$\tag{7e}$$

$$c_t \ \frac{\partial \phi_t}{\partial z} (x, -1) = c_s \ \frac{\partial \phi_s}{\partial y} (x,a)$$

We need one more boundary condition for p at z = -1 to completely define the problem. This boundary condition can be derived from the side layer problem.

2.4   Side Layer

At z = -1 in the core, the transverse current j_z leaves the core, flows unchanged across the side layer and enters the side wall, if $M^{-1/2} << c_s << 1$ [4]. Some of the current entering the side wall flows up the wall (for y > 0) to the top at y = a, z -1. The rest of the current entering the side wall flows in the x direction. However, the side wall current flowing in the x direction must eventually turn to the y direction and enter the top. For c_s comparable to c_t, the current flowing along y in the side wall results in an O(1) electric potential in the side, $\phi_s(x,y)$, having a specific variation with y. Because the core potential at z = -1 has a different specific variation with y, given by equation (2g), there is a jump in the O(1) electric potential across the side layer. The O(1) jump and the $O(M^{-1/2})$ thickness of the side layer result in an $O(M^{1/2})$ voltage gradient, $\partial\phi/\partial z$. At the same time, j_z in the side layer can be at most O(1). As a result, the z component of Ohm's law (1b), $j_z = - \partial\phi/\partial z + uB_y$, dictates that the velocity u be of $O(M^{1/2})$ to balance the $O(M^{1/2})$ voltage gradient $\partial\phi/\partial z$. Thus, in the side layer:

$$u = \beta \ \frac{\partial \phi}{\partial z} \tag{8a}$$

$$\int_{s.l.} u dz = \beta(x) \ [\phi_c(x,y, -1) - \phi_s(x,y)] . \tag{8b}$$

where $\int_{s.l.}$ indicates integration across the side layer. Therefore, the electric potentials in the core and in the side wall determine the volumetric flux per unit length in the y direction. The details of the side layer solution can be ignored, provided we guarantee that the boundary value problem for the side layer variables is well-posed. A sufficient condition for this guarantee is that the side-layer volumetric flux, given by equation (8b), plus the volumetric flux in the core of the flow must be invariant at all cross sections, namely:

$$\frac{\partial}{\partial x} \int_o^a \left\{ \int_{s.l.}^a u\,dz + \int_{-1}^o u_c\,dz \right\} dy = 0. \tag{9}$$

Condition (9) is necessary because the solution for ϕ_t, p and ϕ_s completely determines $w_c(x,y,-1)$, which provides the flow into or out of the side layer. Unless the flow which enters the side layer is the same as that which leaves the core, the side layer problem is not well-posed. Introducing equations (2a, 2g, 4a, 8b) into condition (9) and using the symmetry conditions (7a, b), we obtain the sufficient condition on the core and side wall variables for the side-layer problem to be well-posed:

$$\frac{\partial p}{\partial z}(x,-1) = [\beta^2 + \frac{a^2}{3} \beta'^2]^{-1} \; x$$

$$\left\{ \beta' \phi_t (x-1) - a^{-1} \frac{d}{dx} [\beta \int_o^a \phi_s (x,y)\,dy\,] \right\}. \tag{14}$$

Condition (14) can also be derived by manipulation of the equations governing the side layer variables. These variables satisfy the boundary conditions at the side wall ($u = v = w = 0$, and Eq. (4c)), and match the core variables at the core/side layer interface. Integration of the governing equations across the side layer and use of the boundary conditions at the wall and the matching conditions at the core/side layer interface results in a condition identical to (14).

3.0.   NUMERICAL METHODS

Equations (4a) and (4b) constitute a set of coupled partial differential equations which are solved simultaneously in the rectangular xz domain. Equation (4c) is solved in the rectangular xy domain. The finite difference method is employed. The grid point layout from $y = 0$ to $y = a$ and from $z = -1$ to $z = 0$ at a given x is shown in Figure 2 with staggered grids in the z direction for p and ϕ_t. The finite difference approximations are derived as follows:

3.1   Integrate equation (4a) over a molecule centered at $p_{i,j}$ and equation (4b) over a molecule centered at $\phi_{ti,j}$ (Figure 3). The resulting finite difference equations can be rearranged in the form
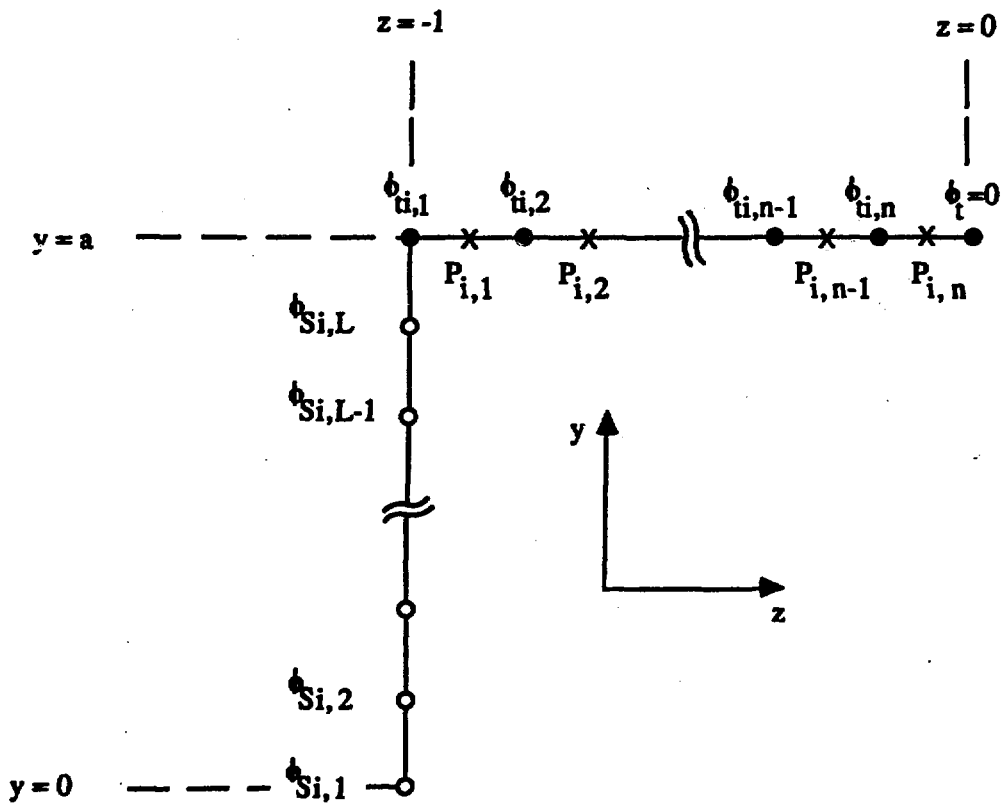
z = -1   z = 0

$\phi_{ti,1}$ $\phi_{ti,2}$ $\phi_{ti,n-1}$ $\phi_{ti,n}$ $\phi_t = 0$

y = a

$P_{i,1}$ $P_{i,2}$ $P_{i,n-1}$ $P_{i,n}$

$\phi_{Si,L}$

$\phi_{Si,L-1}$

y

z

$\phi_{Si,2}$

y = 0 $\phi_{Si,1}$

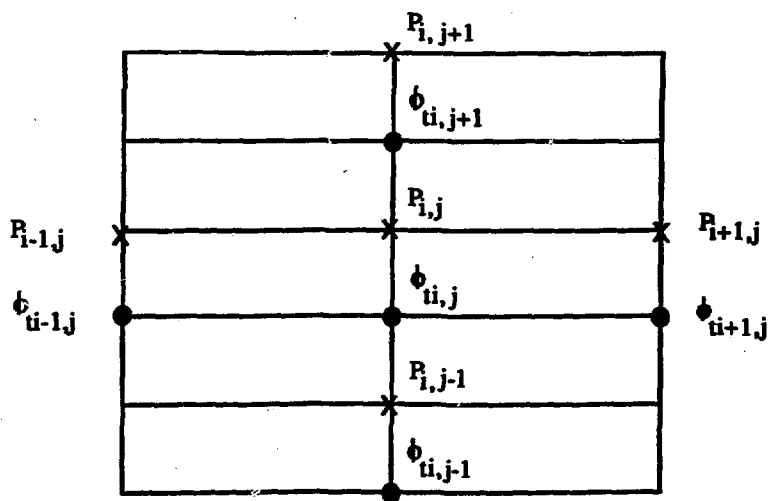**FIGURE 2. MESH LAYOUT AT THE WALLS AT ANY CROSS SECTION**

FIGURE 3. A COMPUTATIONAL MOLECULE FOR $\phi_{ti,j}$ and $P_{i,j}$

$$\begin{bmatrix} a_{11} & a_{12} \\ a_{21} & a_{22} \end{bmatrix} \begin{bmatrix} \phi_{ti,j} \\ p_{i,j} \end{bmatrix} = \begin{bmatrix} b_1 \\ b_2 \end{bmatrix} \tag{15}$$

The coupled equations (4a) and (4b) exhibit rather different characteristics in different regions of β'. For small values of c_t, the equations alternate between elliptic and parabolic forms. In the uniform field region, where β' is small, these equations should be treated as Poisson's equations. They are used to determine $p_{i,j}$ and $\phi_{ti,j}$ due to small perturbations in $\partial\phi/\partial z$ and $\partial p/\partial z$. In the non-uniform field region, β' is large, and for c_t small but finite, these equations give the values of $\partial\phi/\partial z$ and $\partial p/\partial z$ along the characteristic surfaces ($x = $ constant) which in turn determine the values of $\phi_{ti,j}$ and $p_{i,j}$. The simultaneous solution scheme allows the equations' characteristics to change with β. In addition, if equations (4a) and (4b) are solved independently by taking the right-hand-side as known, the truncation error in (4b) would be $(\Delta z)^2/c_t$, and for $c_t \ll 1$, this error would quickly destroy the solution after just a few iterations. In the simultaneous scheme, the truncation error is $(\Delta z)^2$.

3.2   Integrate equation (4c) over a molecule centered at $\phi_{si,k}$ to obtain the general five-point formula expression. If mesh sizes are Δx and Δy, and if $\Delta x > \Delta y$, then the leading truncation error from the Laplacian operator is $(\Delta x)^2$, whereas the truncation error on the right-hand side term is divided by c_s, a small number. The term $\beta(x) \dfrac{\partial p}{\partial z} (x, -1)$ is expanded to higher order so that the truncation error is at least $(\Delta x)^4/c_s$ which will be smaller than $(\Delta x)^2$ everywhere, as long as $c_s > (\Delta x)^2$.

3.3   At $y = a$, $z = -1$, we apply the same scheme as in #1 and #2 to solve for $p_{i,1}$ and $\phi_{ti,1}$. Here the grid point $\phi_{ti,1}$ is at the corner, the molecule around it consists of one part in the xz plane ($z = -1$ to $z = -1 + \Delta z/2$) and the other part in the xy plane ($y = a - \Delta y/2$ to $y = a$). The equation (4b) is integrated over the part in the xz plane, whereas the equation (4c) is integrated over the part in the xy plane; the boundary conditions (7d, e) at the corner are implicitly incorporated because they involve precisely the terms from the integrals of equations (4b, c) evaluated at $z = -1$ and $y = a$. The

coefficients in the system (15) include the integral of $\phi_{si,k}$ from y = 0 to y = a.

For the solution of the systems of finite difference equations, the Gauss-Seidel method was employed with successive over-relaxation (SOR). In general, the problem is intrinsically fast convergent. The relaxation factor may be arbitrarily chosen in the range 1.3 ~ 1.6. However, for very small c (c < 0.01) the relaxation factor should be chosen closer to 1, or even less than 1 (under-relaxation). The iteration was terminated when nodal pressures and potentials were different by less than 0.1% in consecutive steps.

4.0   RESULTS AND DISCUSSION

4.1   Flow Out of a Fringing Magnetic Field

The dimensionless transverse magnetic field model employed is as follows:

$$B_y(x) = \begin{cases} 1 & x \le -x_o \\ \dfrac{1}{2}\left(1 - \sin\dfrac{\pi x}{2x_o}\right) & -x_o \le x \le x_o \\ 0 & x \ge x_o \end{cases} \qquad (16)$$

The field gradients are symmetric about the point x = 0, B_y = 0.5. The field decays to zero from its maximum value of 1 over a distance equal to $2x_o$. The parameter x_o^{-1} characterizes the magnitude of the field gradient. For practical purposes, the tail of $B_y^{-1}(x)$ (near and beyond x_o) is smoothly leveled to a maximum value of 1,000, which corresponds to B_y = 0.001, to avoid overflow/ underflow in the computations. Results presented here are for x_o = 3, c_s = c_t = 0.02, a = 1. They are shown in the range x = -6 (B_y = 1) to x = 2 (B_y = 0.07). As the field becomes too small the local Hartmann number and interaction parameter become small and the inertialess, inviscid assumptions are no longer valid.

Figures 4 and 5 show the electric potential at the top wall and side wall, respectively, divided by the local magnetic field. If the flow were locally fully developed everywhere, all the curves in these figures would coincide with the one shown at x = -4.2. In reference to equation (2g), the electric potential in the fluid will exhibit
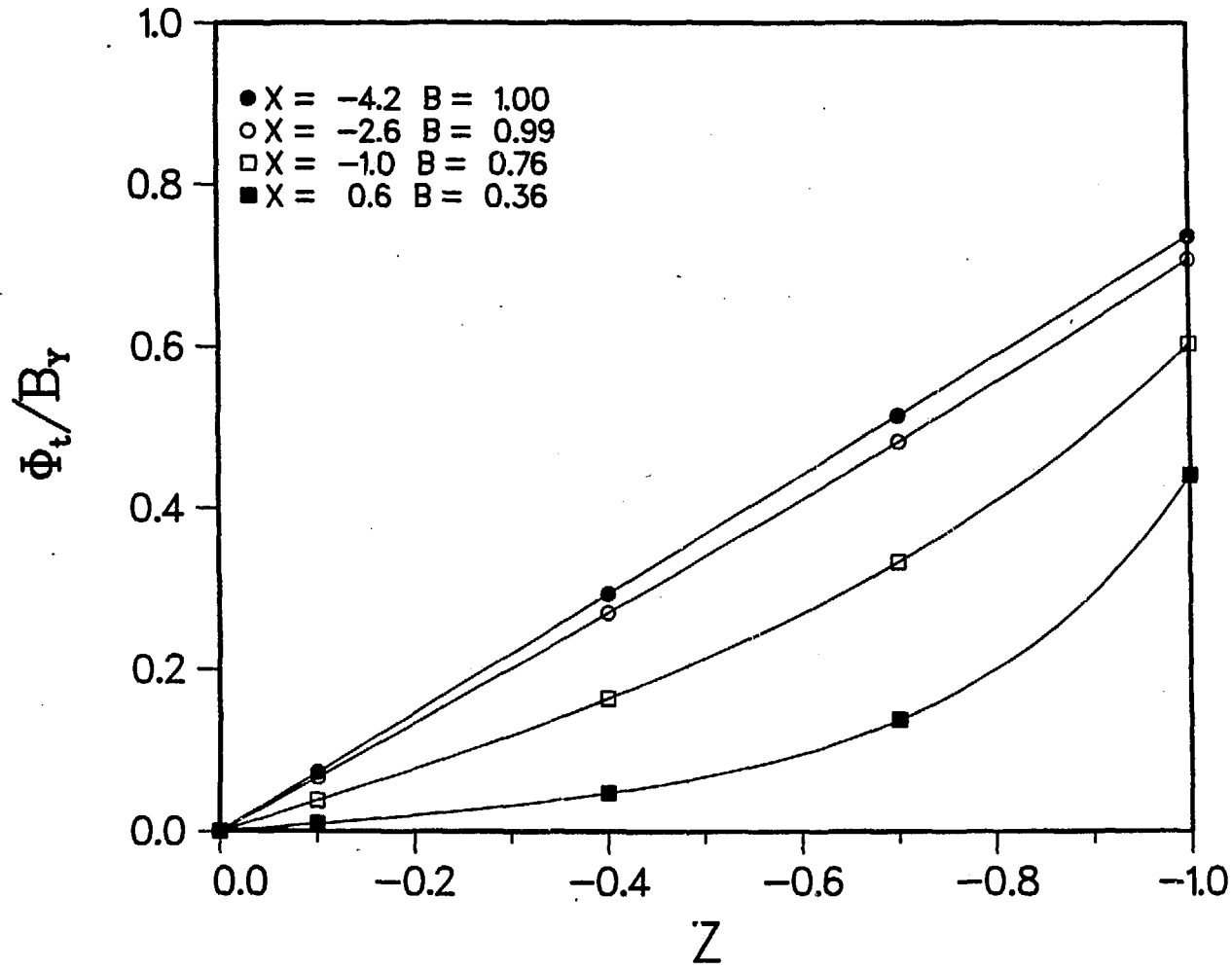
13

14

FIGURE 4
TOP WALL ELECTRIC POTENTIAL PROFILES
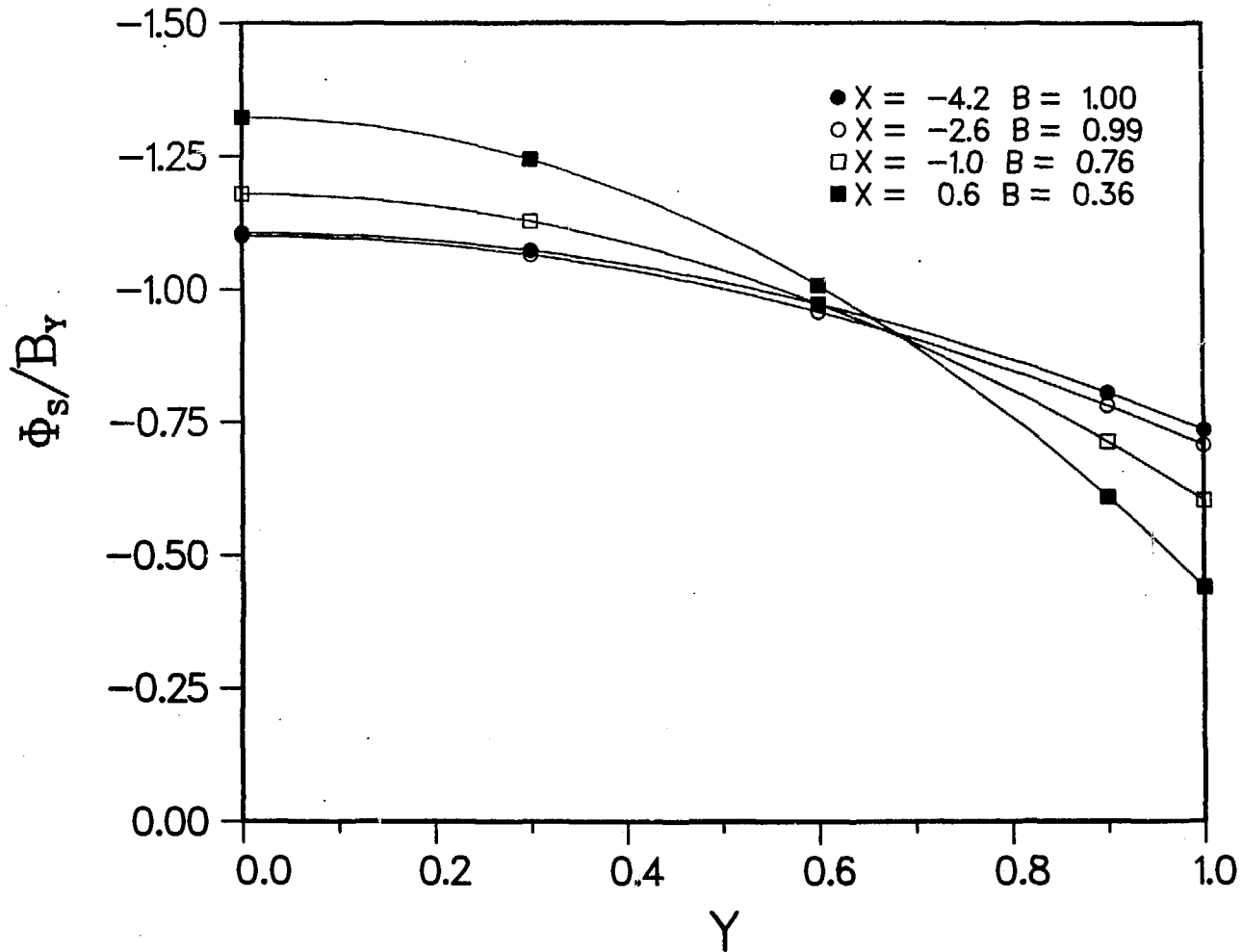DIVIDED BY THE LOCAL DIMENSIONAL MAGNETIC FIELDS

FIGURE 5
SIDE WALL ELECTRIC POTENTIAL PROFILES
DIVIDED BY THE LOCAL DIMENSIONAL MAGNETIC FIELDS

similar behavior as in Figure 4. The axial potential differences drive axial electric currents in the fluid and in the walls in the ± x direction for z $\gtrless$ 0. The slopes of the curves in Figure 4 are proportional to the local velocity. At x = -4.2 where the flow is fully developed, the velocity is uniform across z. As the flow evolves downstream (increasing x), the 3-D effects cause the velocity to increase near the side and decrease elsewhere. The axial velocity profiles in the y = 0 plane and at various cross sections are shown in Figure 6. A companion plot of axial velocity distributions along x, at various z locations, is shown in Figure 7. For fully developed flow, the fraction of the total volumetric flux that flows inside the two side layers is given by: $[1 + 3c_s$ $(1/ac_t + 1/a^2)]^{-1}$. It can be deduced from Figure 7 that 3-D effects increase this fraction, leaving a slowly moving region in the center.

Figure 8 shows the variation of pressure at z = 0 and z = -1. In contrast to locally fully developed flow for which pressure is uniform at each cross section, here the pressure at z = 0 is smaller than that at the side. The difference arises from the interaction between axial current and magnetic field.

One of the more important variables pertinent to fusion reactor blanket design is the axial pressure gradient, which, when integrated over a duct length of interest, yields the overall MHD pressure drop. Miyazaki [5] asserted that the total pressure drop in a nonuniform field could be obtained by integrating the pressure gradient formula derived for fully developed flow. By coincidence, their experimental results supported this assertion for the cases they investigated. In general, this is not true. Depending on the wall conductance ratio and the rate of change of magnetic field, the overall pressure drop calculated by assuming locally fully developed flow could underestimate the actual pressure drop by a few percent to perhaps as much as one hundred percent. Figure 9 shows our numerical results for the pressure gradient at z = 0 and z = -1. The dashed curve gives the locally fully developed pressure gradient which is proportional to the square of the local field strength with a proportionality constant given by $K = \left(1 + \frac{a}{c_t} + \frac{a^2}{3c_s}\right)^{-1}$. It is obvious that with 3-D effects, the proportionality factor is not constant along x or z. The overall pressure drop from x = -6 to x = 2 given by the numerical analysis is 0.0932. A locally fully developed hypothesis yields a figure of 0.0754, an underestimate of the pressure drop of 19%.
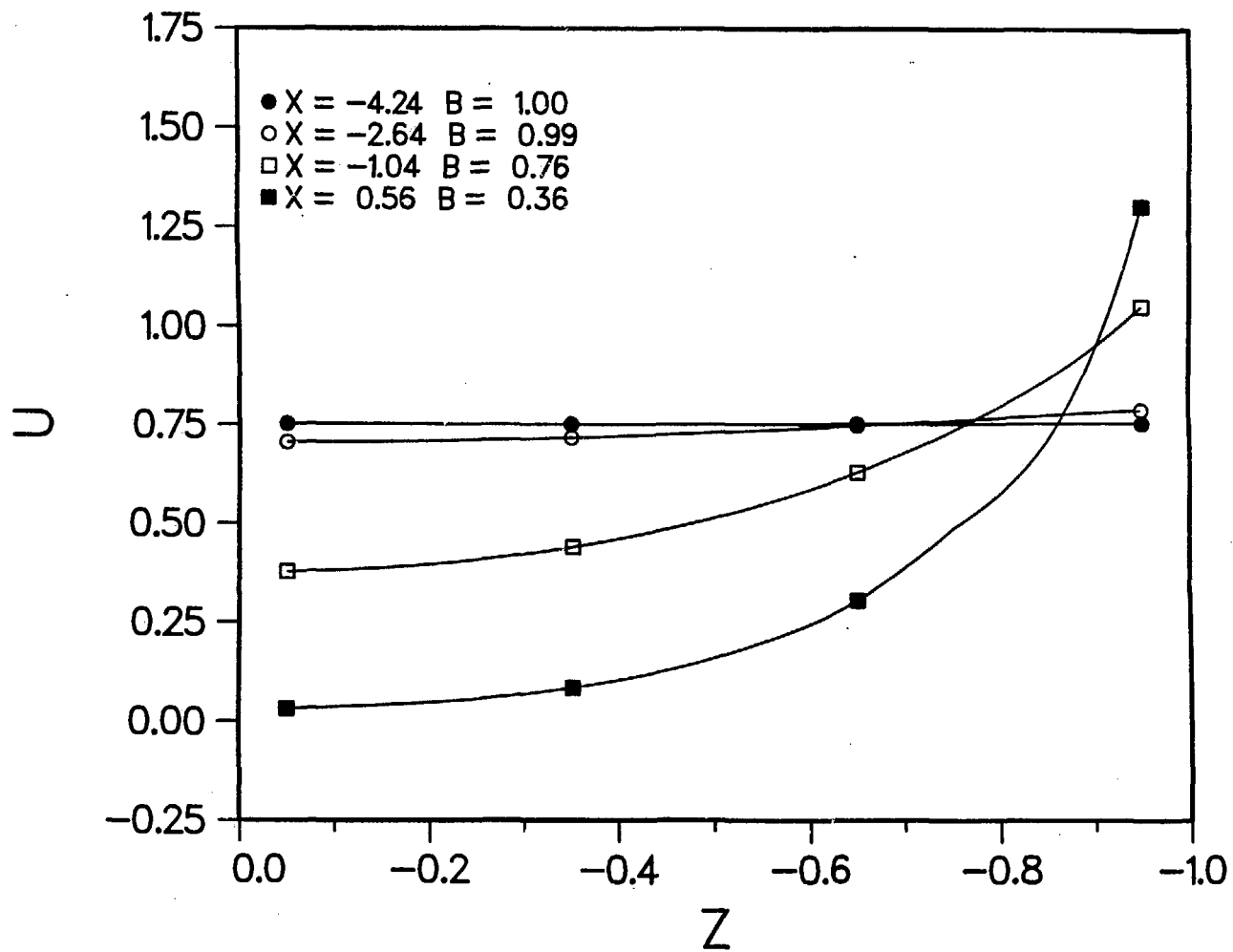
16

FIGURE 6
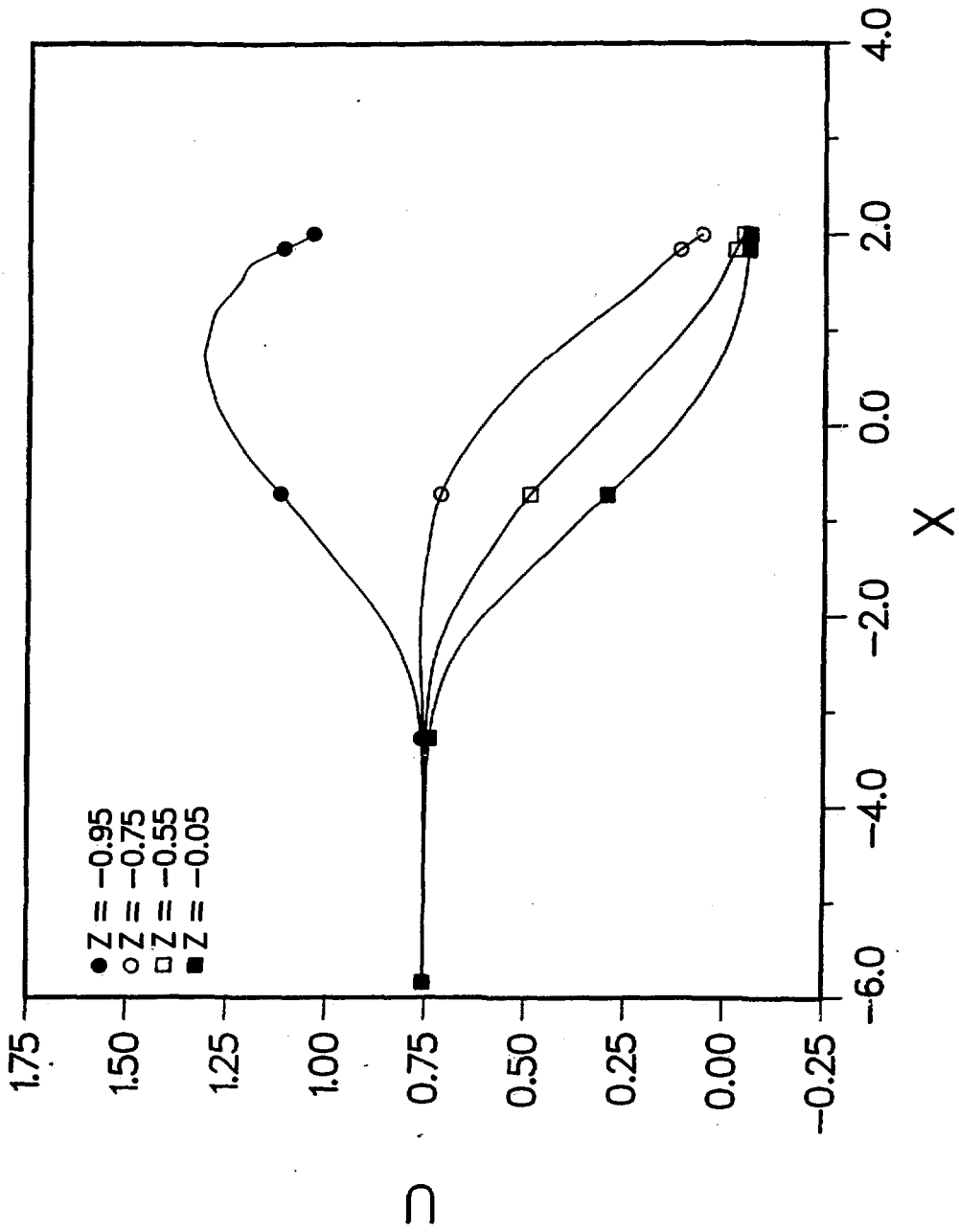**AXIAL VELOCITY PROFILES IN MIDPLANE (y = 0) AT VARIOUS CROSS SECTIONS**

FIGURE 7
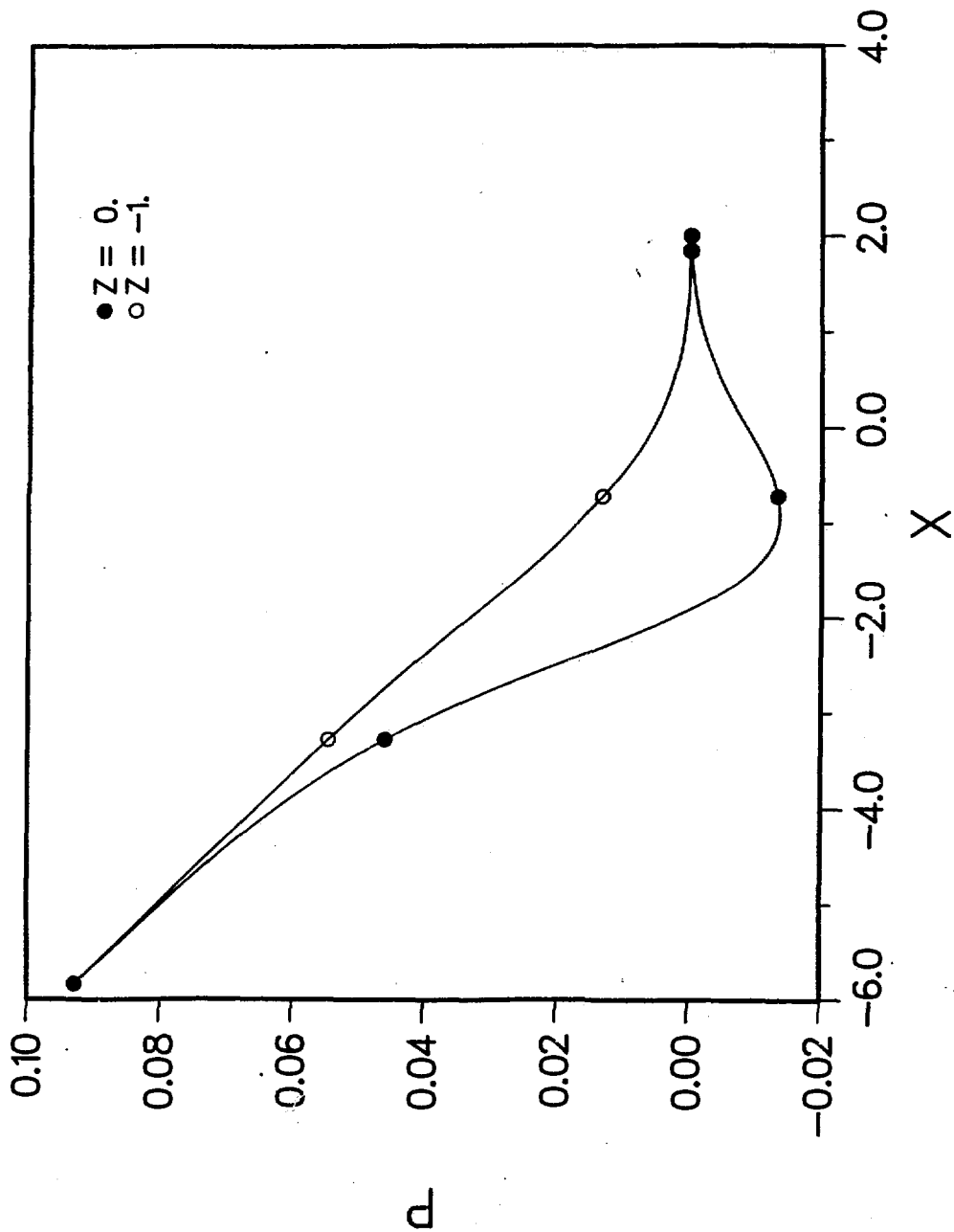AXIAL VELOCITY PROFILES IN MIDPLANE (y = 0) AT VARIOUS z LOCATIONS

Legend:
● Z = −0.95
○ Z = −0.75
□ Z = −0.55
■ Z = −0.05

FIGURE 8

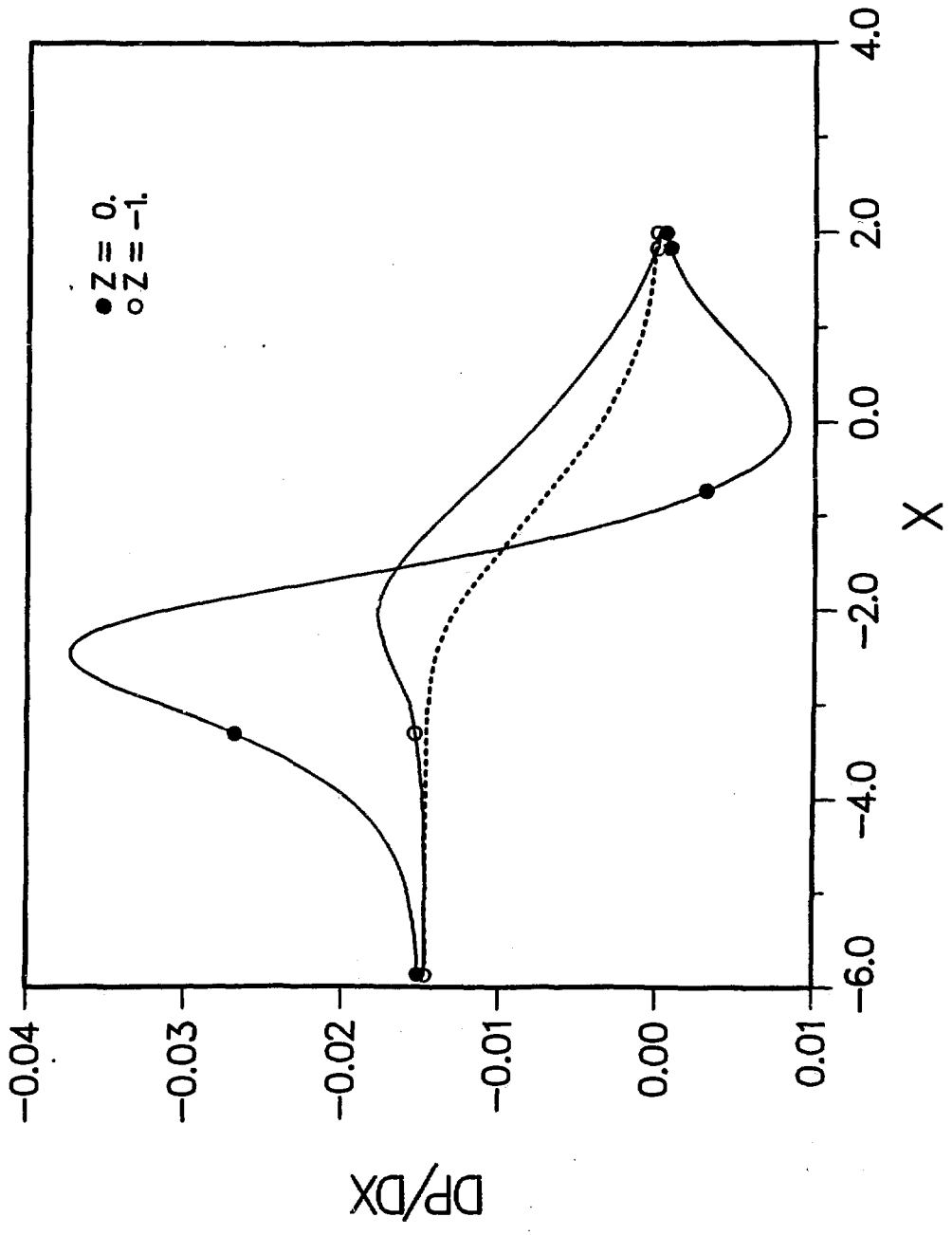**PRESSURE VARIATIONS AT THE CENTERLINE (z = 0) AND AT THE SIDE (z = -1)**

FIGURE 9

AXIAL PRESSURE GRADIENT AT THE CENTERLINE (z = 0) AND AT THE SIDE (z = -1)

A parametric study was performed to investigate the additional pressure drop resulting from 3-D effects, Δp_{3-D}, for a square duct with the same conductance ratios for all walls. The values of c varied from 0.02 to 0.2, and the values of x_o considered were 2, 3 and 4. Results are plotted in Figure 10 which presents Δp_{3-D} a function of $C^{1/2}$. Notice that Δp_{3-D} increases linearly with $c^{1/2}$ for c < 0.1 which covers the range of interest to most fusion blanket conduits. The total pressure drop is then given by

$$\Delta p = \Delta p_{fd} + \Delta p_{3-D} \tag{17}$$

where

$$\Delta p_{fd} = K \int_{x_1}^{x_2} B_y^2(x)\, dx \tag{18}$$

and

$$\Delta p_{3-D} = kc^{1/2} \quad \text{for } c < 0.1 \, . \tag{19}$$

The values of k are also tabulated in Figure 10.

The results in Figure 10 are quantitatively valid for a square duct with the same conductance ratios on all four walls. The results are also valid qualitatively for different cross sectional aspect ratios and different wall conductances for the top and side walls. If a detailed answer for a particular choice of the parameters a, c_t, c_s and x_o is required, the numerical solution reported here will simply have to be repeated for the desired set of parameters. This is a straight forward task. Covering the entire range of possible a's, c_s's, c_t's, and x_o's is outside the scope of this paper. Nonetheless, physical reasoning can be used to indicate the way in which the results of Figure 10 would vary with the aspect ratio "a", and the ratio c_t/c_s. The formulae given in this section indicate that the fraction of the total flow, carried by the side layers in fully developed flow, increases with increasing "a" or c_t/c_s. Consequently, the velocity in the core would decrease as would the induced transverse voltages which are proportional to the core velocity. It follows that the axial currents, which are driven by axial voltages differences, would also decrease as would the 3-D perturbation. Therefore, an increase in "a" or c_t/c_s decreases the additional pressure drop caused by 3-D effects. The quantiative aspects of this effect would, of course, depend on x_o or, more generally, on the magnetic field distribution.
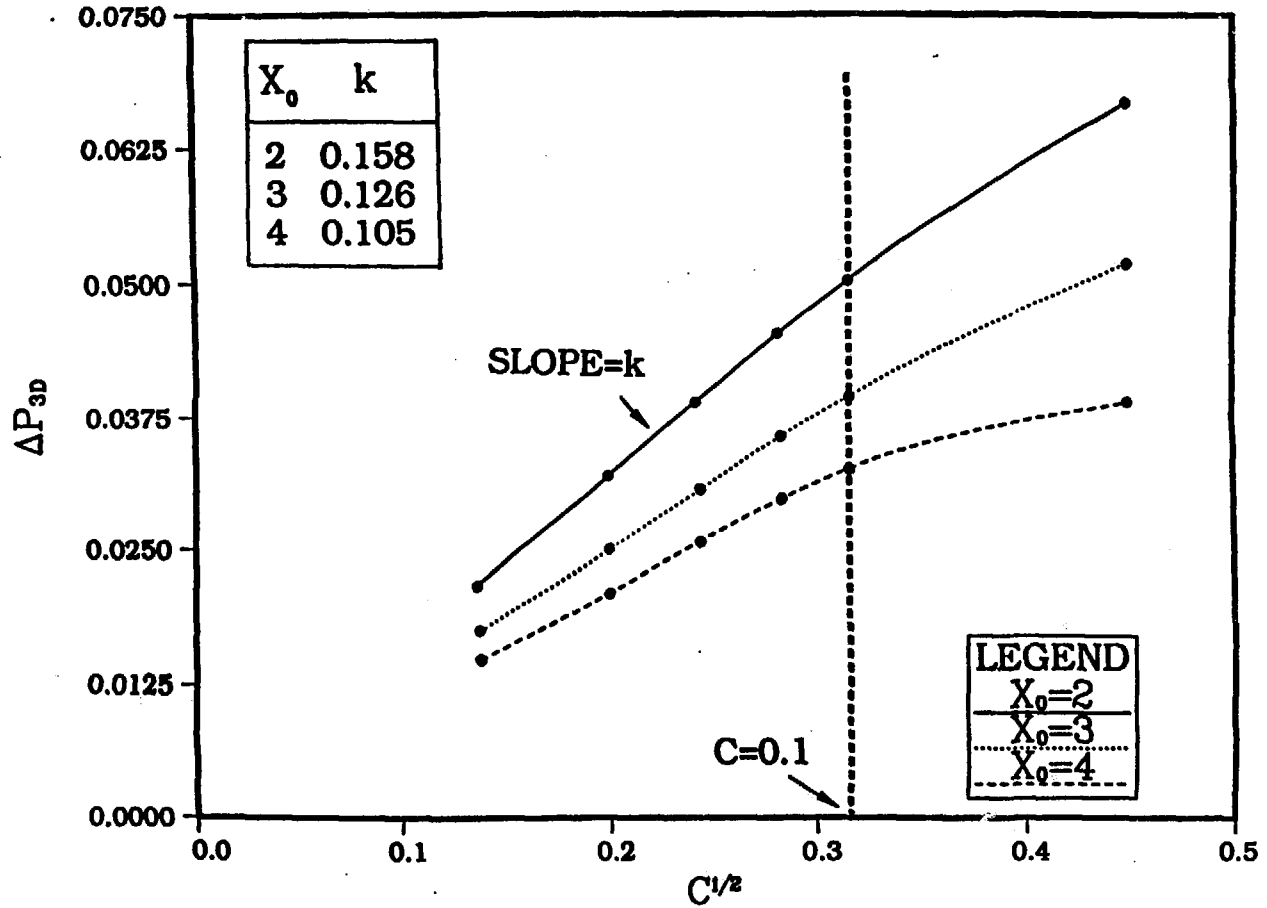
FIGURE 10. ADDITIONAL PRESSURE DROP TO THE 3-D EFFECT

4.2 Comparison with Experiments

An experimental facility, ALEX, described in detail elsewhere [2], was built at Argonne National Laboratory to study liquid metal MHD phenomena relevant to fusion blanket engineering. A recent test series involved a square duct made of stainless steel. Its width, length, and wall thickness were 8.8 cm, 610 cm, and 0.66 cm, respectively. The working fluid was NaK. The wall conductance ratio was 0.07. The transverse magnetic field was applied to the test section by a magnet which can generate a maximum field of 2.1 T. The peak Hartmann number and a typical interaction parameter were 6,400 and 100,000. These values are close to and in some cases overlap with the values prevailing in a fusion reactor. Measurements at various axial locations include axial and transverse pressure differences, axial and transverse potential differences, and axial velocities. A full description of the test series and complete analysis of experimental data for the numerous test cases will be presented in a future paper. Typical results are given in Reference 3. Within the scope of this paper, we show only a few representative results for comparison with the numerical predictions.

Figure 11 compares the measured dimensionless average axial pressure gradient in the fluid at z = -1 with the numerical results. The $B_y(x)$ used for these numerical results are the values actually measured in the experiment, normalized by the uniform field value. The average pressure gradient is calculated as $\Delta p/\Delta x$, where Δp is the pressure drop over a distance Δx (in the experiment, Δx = 7.6 cm in experiment). The upper data curve is for $N = 1.26 \times 10^5$ and M = 5800. The lower one is for N = 540 and M = 2900. The quality of the agreement between code predictions and experimental data at high and low N seems to be similar, indicating that, the present numerical analysis may be valid for N as low as 500 or perhaps lower.

Figure 12 shows comparison the variation of the transverse pressure difference, p (x, -1) - p (x, 0) with the axial position. As indicated earlier, a non-zero value indicates 3-D MHD effects.

The axial currents in the side wall interact with the strong magnetic field to produce a pressure drop across the side wall, along the liquid-metal-filled hole in the side wall through which the pressure at z = -1 is measured. The measured pressure difference is inevitably modified by the pressure difference across the side wall. To
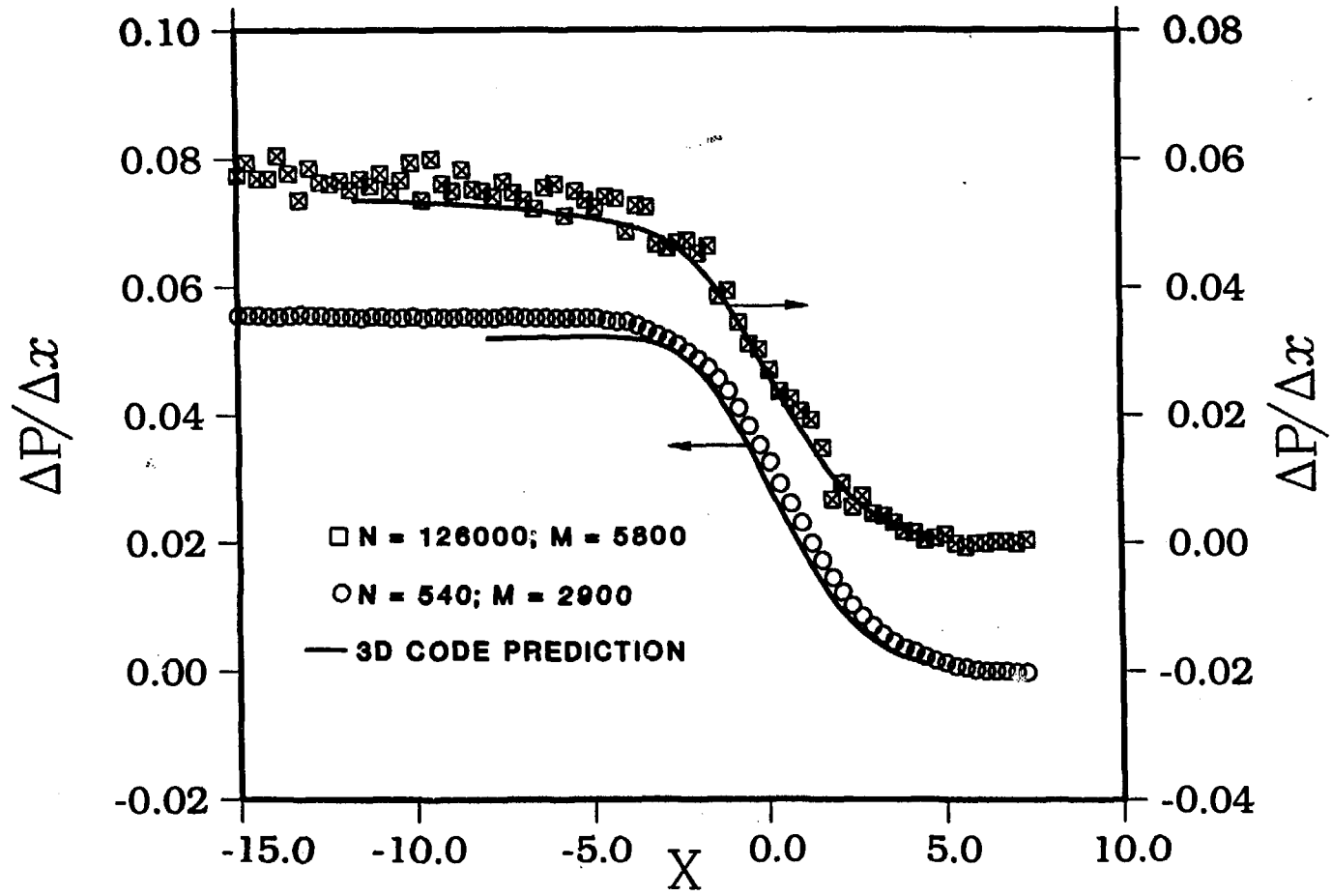
FIGURE 11
COMPARISON BETWEEN EXPERIMENTS AND CODE PREDICTIONS
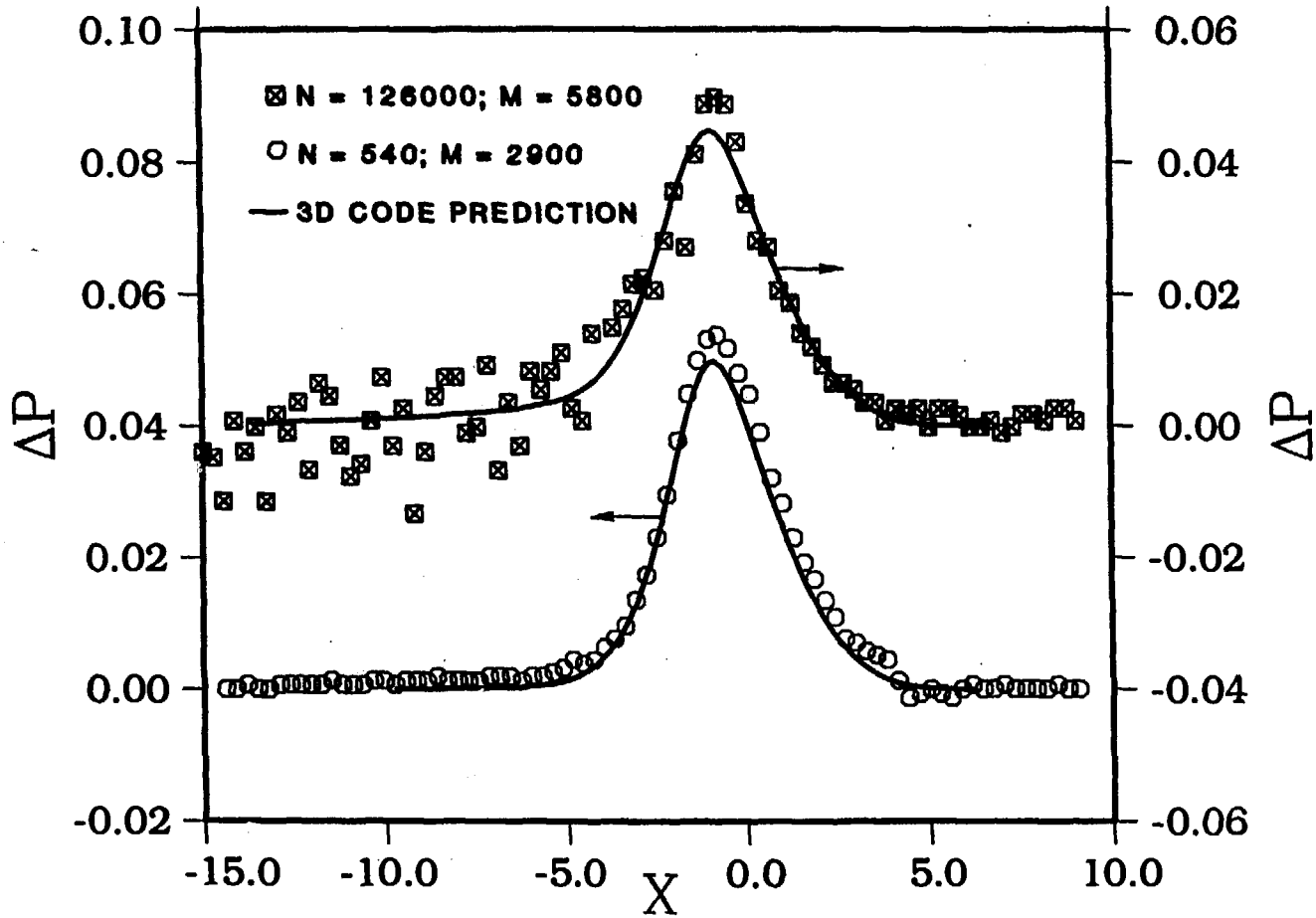FOR THE AVERAGE AXIAL PRESSURE GRADIENTS AT z = -1

FIGURE 12
COMPARISON BETWEEN EXPERIMENTS AND CODE PREDICTIONS
FOR THE AXIAL TRANSVERSE PRESSURE DIFFERENCE, p (x, -1) - p (x, 0)

compare appropriately the numerical predictions with experimental results, the numerical results shown in Figures 11 and 12 also include the effect of the pressure drop across the side wall.

Figure 13 compares the axial voltage difference at the side wall in the y = 0 plane. In the nonuniform field region, some of the transverse current that leaves the core and enters the side flows up the side wall to the top. The rest of the current flows in the axial direction in the side wall, which gives rise to these axial voltage differences. The voltage differences were measured over an axial distance of 7.6 cm.

4.3 Gradually Varying Magnetic Field

In the past, for the cases in which the magnetic field changes gradually over the length of the duct, such as the inlet and outlet coolant ducts of the inboard of a blanket module, the flow was generally assumed to be fully developed in calculating the pressure drop. At present, accurate criteria for establishing whether a variation of the field is sufficiently gradual do not exist. In this section we attempt to shed some light on this issue for a square duct with uniform wall thickness.

In a tokamak, the toroidal field varies as A/R, where A is a constant and R is the distance from the center of the torus. We formulate the problem as follows: Let r_1 and r_2 be the dimensionless radial positions of two locations on a duct which lies along the radial direction of the torus; r is nondimensionalized by the half-width of the duct, L. The magnetic field is normalized by A/r_1 so that the dimensionless field varies from 1 at r_1/r to $B_\omega = r_1/r_2 < 1$ over the length of the duct $l = r_2 - r_1$. Assume that the duct extends beyond r_1 and r_2 where the conditions for fully developed flow apply. At a given B_ω, a decreasing value of l corresponds to either an increasing L or a decreasing duct length for a fixed cross section, hence a larger magnetic field gradient. In either case one would expect 3-D effects to increase. It is important to determine the range of l for which 3-D effects are important and a 3-D analysis is required.

When 3-D effects exist, the axial velocity near the side increases from its fully developed value, whereas near the centerline it decreases. The difference between the maximum and minimum velocities, ΔU, divided by U_o is taken as an indication of the extent of 3-D effects. The values of B_l considered are 0.6 and 0.4; l is varied in the
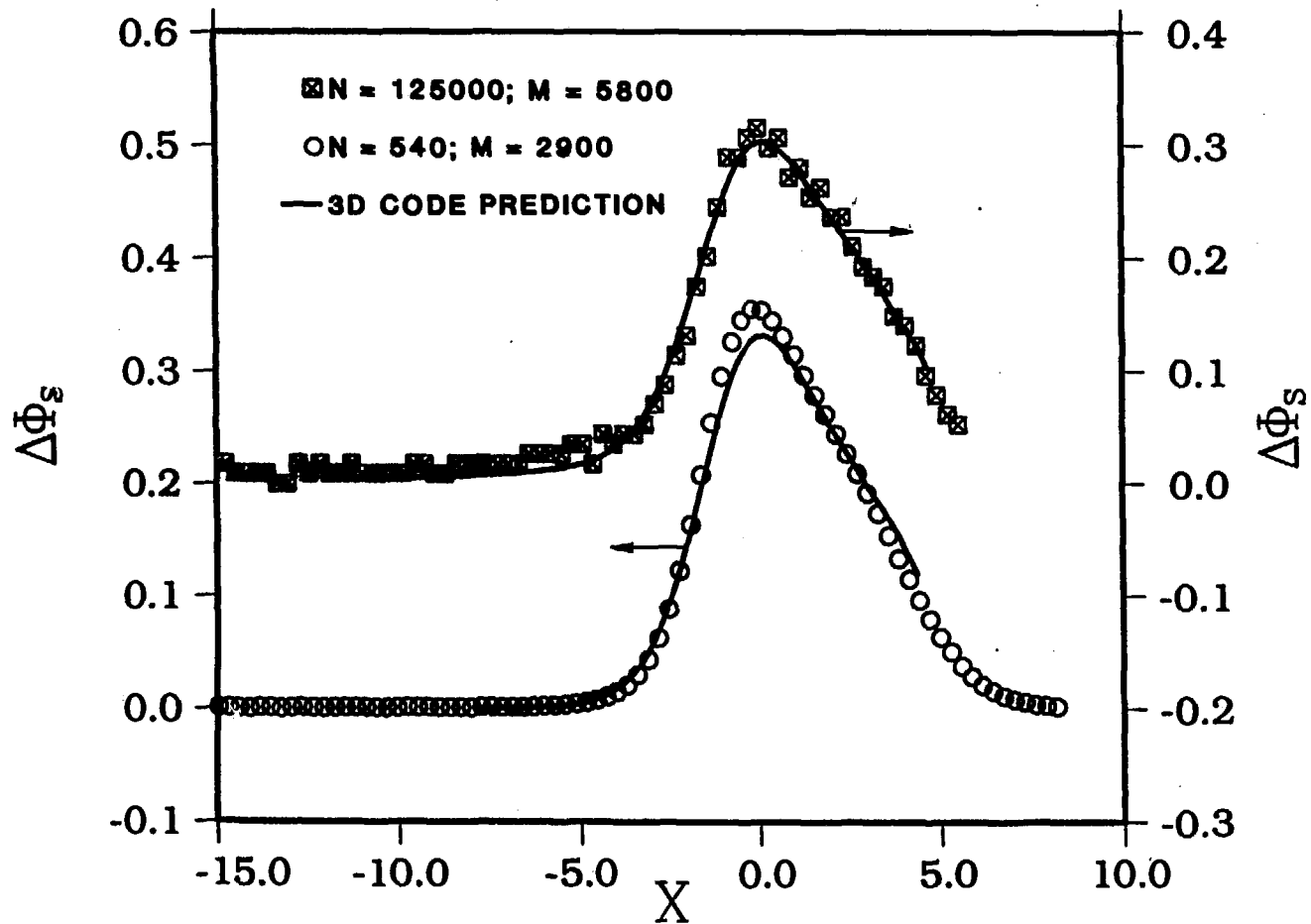
FIGURE 13
COMPARISON BETWEEN EXPERIMENTS AND CODE PREDICTIONS
FOR THE AXIAL VOLTAGE DIFFERENCES AT THE SIDE WALL IN THE y = 0 PLANE

range 5 - 20. Results for $c = 0.02$ and 0.1 are shown in Figure 14. As expected, 3-D effects increase when any one of the following variables decreases: c, l, and B_l. When $\Delta U/U_o$ is less than 10% the 3-D effects are generally small enough to assume locally fully developed conditions. In the cases investigated, this corresponds to $l \geq 20$. For the BCSS liquid metal blanket[1], the values of the parameters for the inlet conduits were $B_l = 0.6$, $c = 0.01$, and $l = 40$, so any errors associated with the fully developed flow assumption made in that study would be minimal.
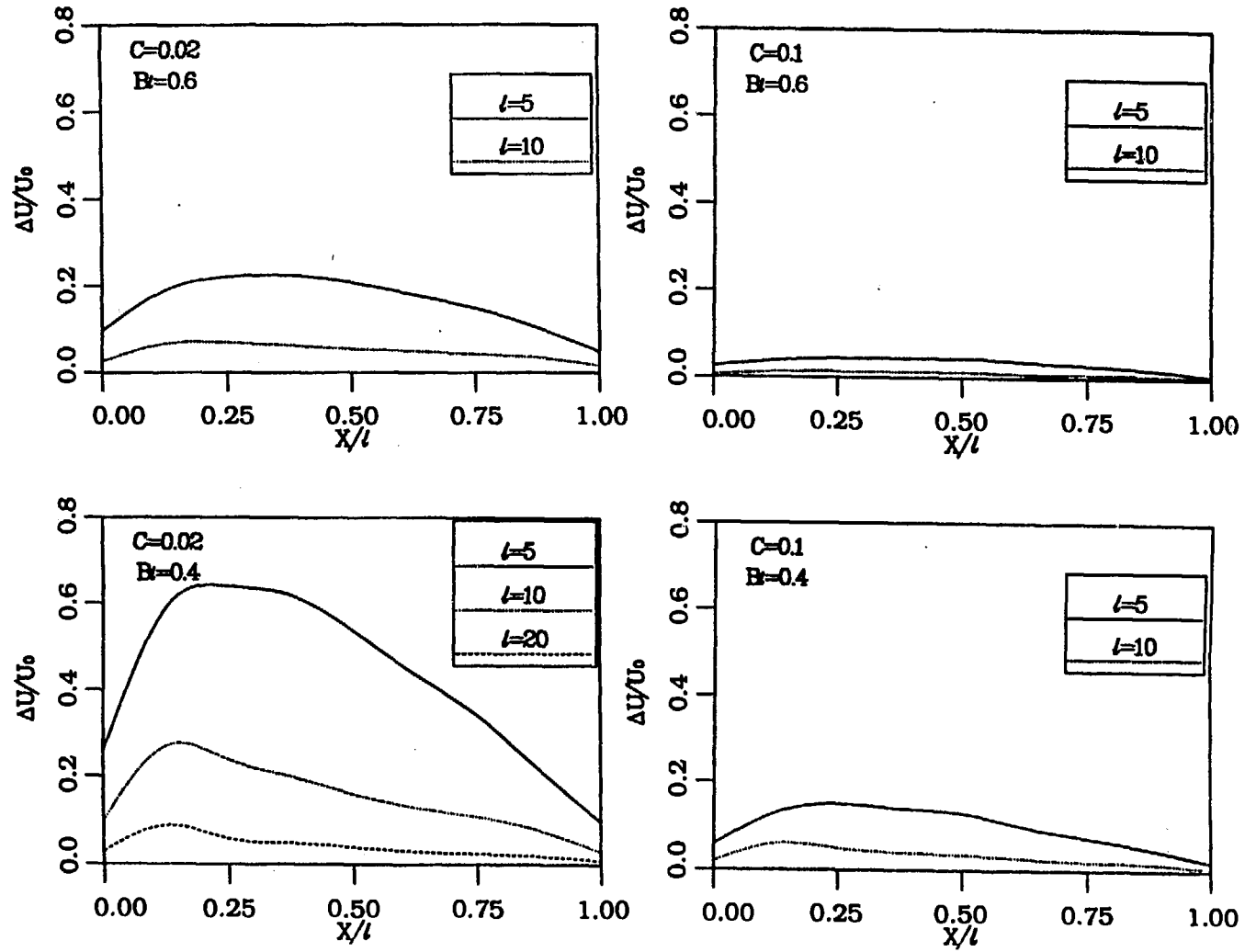
FIGURE 14
VARIATION OF THE DIFFERENCE BETWEEN AXIAL VELOCITIES NEAR THE SIDE
AND NEAR THE CENTERLINE OVER THE LENGTH l
(___ l = 5, - - - - l = 10, ... l = 20).

ACKNOWLEDGMENTS

REFERENCES

1. D. L. Smith et al., Blanket Comparison and Selection Study - Final Report, Argonne National Laboratory Report ANL/FPP 84-1 (1984).

2. C. B. Reed, B. F. Picologlou, and P. V. Dauzvardis, "Experimental Facility for Studying MHD Effects in Liquid-Metal-Cooled Blankets", Fusion Technology, Vol. 8, Part 2A, pp. 257-263 (July 1985).

3. C. B. Reed, B. F. Picologlou, T. Q. Hua, and J. S. Walker, "ALEX Results - A Comparison of Measurements from a Round and a Rectangular Duct with 3-D Code Predictions", IEEE 12th Symposium on Fusion Engineering, (October 1987).

4. J. S. Walker, "Magnetohydrodynamic Flows in Rectangular Ducts with Thin Conducting Walls. Part 1. Constant-Area and Variable-Area Ducts with Strong Uniform Magnetic Fields," Journal de Mecanique Theorique et Appliquee, Vol. 20 (1981).

5. K. Miyazaki, S. Inoue, N. Yamaoka, T. Horiba, and K. Yokomizo, "Magnetohydrodynamic Pressure Drop of Lithium Flow in Rectangular Ducts," Fusion Technology, Vol. 10, Part 2A (November 1986).

Internal:

H. Attaya	D. Gruen	C. Reed
C. Baker	A. Hassabein	D. Smith
E. Bennett	T. Hua (10)	H. Stevens
M. Billone	A. Hull	D. Sze
J. Brooks	C. Johnson	L. Turner
Y. Cha	A. Krauss	T. Yule
O. Chopra	Y. Liu	FPP Files (25)
R. Clemmer	B. Loomis	ANL Contract File
D. Ehst	S. Majumdar	ANL Libraries
K. Evans	R. Mattas	ANL Patent Dept.
P. Finn	B. Picologlou	TIS Files (3)
Y. Gohar	R. B. Poeppel	
L. Greenwood	K. Porges	

External:

DOE-OSTI for Distribution per UC-420 (37)
Manager, Chicago Operations Office
M. Abdou, University of California – Los Angeles
J. Anderson, Los Alamos National Laboratory
L. Barleon, KfK, Germany
J. Barlit, Los Alamos National Laboratory
W. Bauer, Sandia Laboratories
S. Berk, Office of Fusion Energy
L. Bromberg, Massachusetts Institute of Technology
J. Clarke, Office of Fusion Energy
M. Cohen, Office of Fusion Energy
D. Cohn, Massachusetts Institute of Technology
R. Conn, University of California – Los Angeles
J. Crocker, EG&G Idaho, Inc.
J. Davis, McDonnell Douglas Astronautics Company
S. Dean, Fusion Power Associates
R. Dowling, Office of Fusion Energy
P. Dunn, University of Notre Dame
C. Flanagan, Oak Ridge National Laboratory
H. Forsen, Bechtel National Inc.
H. Furth, Priceton Plasma Physics Laboratory
P. Gierszewski, Canadian Fusion Fuels Technology Project
J. Gordon, TRW, Inc.
R. A. Gross, Columbia University
G. Haas, Office of Fusion Energy
R. Hancox, Culham Laboratory
C. Henning, Lawrence Livermore National Laboratory
D. Holland, EG&G Idaho, Inc.
N. Hoffman, Energy Technology Engineering Center
G. Hollenberg, Hanford Engineering Development Laboratory
M. Hsiao, Pennsylvania State University